Utilizing Mobile Doppler Wind Lidar Observations and Idealized Modeling to Understand the Characteristics of a Density Current's Vertical Velocity Field

Principal Investigator: Nolan Meister[1]
Principal Investigator: James Cuellar[1]
Co-Investigator: Dr. Elizabeth Smith[2]
Co-Investigator: Dylan Reif[1]

[1]University of Oklahoma, School of Meteorology
[2]NOAA/OAR/National Severe Storms Laboratory

1. Abstract

Density currents associated with thunderstorm outflow are a well-documented and well-researched phenomenon; however, how the vertical velocity near the density current interface interacts with the surrounding environment is not well-understood. Doppler mobile lidar and other high-resolution observations from similar tools have provided more insight into the complexities of vertical motions in and within the vicinity of density currents. While observations of notable updrafts preceding outflow boundaries have been cataloged, idealized simulations of these updrafts are not common in the literature. This lack of research addressing these areas of ascent neglects a vital aspect of the evolution of density currents. This study explores the sensitivity of density current features to density current strength (potential temperature perturbation) and environmental properties (wind shear and lapse rate). Our simulations noted that antecedent updraft and ascent above the density current are maximized in a low-shear and low-static stability environment. In contrast, a high-shear and high-static stability environment led to the most modest vertical motions associated with the passage of the density current. The vertical motions within the vicinity of a density current are important to the maintenance, duration, and propagation of the parent thunderstorm along with the initiation of new convection. Understanding what effect environmental variables have on the vertical velocity ahead of and above the density current can improve our comprehension of processes around the parent thunderstorm including significant hazards associated with these phenomena.

2. Introduction

Thunderstorm outflow is a well-known and well-researched phenomenon. It occurs within the mature stage of a convective storm when rain-cooled, dense air rushes to the surface then outward away from the parent thunderstorm. This creates a boundary separating the rain-cooled, denser air from the surrounding environment. In this way, thunderstorm outflow behaves as a density current. This phenomenon was first documented by Byers and Braham (1949); however, until the widespread implementation of Doppler radar, observations and research of the evolution of thunderstorm outflow were confined to in-situ observations and laboratory experiments. When Doppler radar was implemented on a broader scale in the 1970s (Crum and Alberty 1993), process understanding of thunderstorm outflow blossomed with this new observational capability. Soon three-dimensional idealized and conceptual models were developed (e.g. Charba 1974; Goff 1976), which, with time, have become more complex as observational and numerical tools have improved.

Thunderstorm outflow includes both cold pool outflows and rear-flank downdraft (RFD) outflows, a phenomenon apparent in mature supercell thunderstorms. These two types of thunderstorm outflow have some common characteristics. As these outflow density currents propagate along the surface, they displace warm, ambient air upward. After these outflow density current pass, turbulent vertical motions, pressure and temperature perturbations, and pronounced wind shifts are commonly noted. One of the major differences between cold pool and RFD outflows is the magnitude of the vertical static stability perturbations following passage of the boundary. Both cold pools and RFDs are associated with an increase in static stability; in other words, a negative potential temperature perturbation upon passage of the boundary. However, cold pools have a larger negative potential temperature perturbation associated with boundary passage than RFDs do (Charba 1974; Markowski 2002). This difference causes notable changes in aspects of outflow boundary structure and evolution along with modification of the environment after boundary passage. Understanding ambient environment parameters that influence the structure and evolution of both cold pools and RFDs will help in comprehending aspects of vertical motions in and around the boundary.

To begin to understand the complex processes associated with outflows, simulation approaches have long been utilized, complementing observation-based studies. Early idealized simulations were developed based on observations from laboratory experiments (e.g. Simpson 1969). As observational capabilities increased (e.g., Doppler radar), simulations of density currents included new information from these observations; however, most simulations remained idealized due to the complexities of the physical environment that outflows often occur within and limitation of computing resources. As computational abilities improved, grid spacing within these models decreased changing how density currents were represented within idealized models, as the simulations were able to resolve finer details that coarse grids could not (e.g. Droegemeier and Wilhelmson 1987; Straka et al. 1993). Modern idealized models can allow for simulations on fine grid spacings to evaluate thunderstorm outflow and the parameter space which may control outflow characteristics.

Data collected on thunderstorm outflow today are still taken via in-situ observations and doppler radar; however, there has been a substantial increase in the spatial coverage of these observations. Also, mobile Doppler radar and Doppler lidar used in field research campaigns across the United States have provided fine, detailed observations of kinematic processes within the boundary layer, including thunderstorm outflow. These novel and targeted observations of boundary layer processes have allowed us to observe much finer features than previous methods. As our simulation capabilities increase to allow for high-resolution modelling, analysis of such observations and comparison to simulation data to improve process understanding is critical.

The evolution of density currents generated by thunderstorms can give us real-time context about the nature of the parent thunderstorm itself. For example, Gunter (2015) and Hutson et al. (2019) showed that the inclination of the density current interface may provide a way to implicitly identify buoyancy perturbations within cold pools, which is an important but difficult to observe parameter for determining tornado potential. Thunderstorm outflows are also important to initiation of new convection and convection maintenance (Droegemeier and Wilhelmson 1985a; Rotunno et al. 1988), and may even contribute directly to tornadogenesis via strong localized convergence at the outflow boundary (Wilson 1986; Lee and Wilhelmson 1997b). Numerical weather prediction also reaps the benefits from detailed studies of

thunderstorm outflow. Outflows are crucial factors in boundary layer evolution, but inherently difficult to represent in weather prediction models due to their scale and complex interactions with the surrounding environment. Better understanding of the conceptual model of thunderstorm outflow and its place in the conceptual model of a parent thunderstorm is important for improving numerical models, forecasts, and warnings.

This research seeks to compare modern state-of-the-art idealized numerical simulations of thunderstorm outflow associated density currents to novel observations collected during a spring 2019 field campaign in the United States Great Plains. More specifically, we seek to understand how cold pool outflow or RFD characteristics influence the antecedent updraft and the subsequent vertical motion(s) as the associated density current boundary passes. Vertical motions associated with density currents are imperative in the modification of the surrounding environment which can impact duration and propagation of the parent thunderstorm or even initiate new convective cells. Also, characteristics of the surrounding environment, such as variations in vertical static stability and low-level wind shear have been shown to create differences in outflow boundary structure and evolution (Bryan and Rotunno 2014b; Hutson et al. 2019). Several studies have previously considered outflow boundaries and their importance in a variety of contexts. The combination of novel field observations and the modern numerical model used in this work allows us to visit new ideas associated with thunderstorm outflow.

Turbulent vertical motion within regions of outflow boundaries was first documented in laboratory experiments and in conceptual models of thunderstorm outflows. Supported by the eventual increase in observational data, Wakimoto (1982) found the continuity equation can be applied to accurately estimate the evolution and structure of thunderstorm outflow. The first direct measurements of vertical velocities before and after boundary passage were documented by Martner (1997). Martner found vertical motion near the boundary to have a speed of 10 m s^{-1}. The existence of a strong updraft along the leading edge of outflow boundaries was supported by Reif and Bluestein (2019) where a 13 m s^{-1} updraft was recorded prior to boundary passage during a mesoscale convective system (MCS) event in 2015. Modeling this antecedent updraft has been challenging though. Even with smaller grid spacing in idealized simulations, which have been proven to improve how thunderstorm outflow is modeled, studies as recent as Seigel

and van den Heever (2012) still have idealized models with negligible vertical motion within the antecedent updraft.

This research project will utilize recent novel field observations and state-of-the-art numerical tools to examine the relationship between density current structure and the updraft found within a storm's inflow region. In doing so, we will contribute to a better understanding of boundary layer behavior in and around thunderstorms and improve the overall conceptual model of thunderstorm outflow. The specific research questions governing this project are as follows:

- How do environmental factors such as vertical variations in static stability and vertical wind shear impact the magnitude of an outflow's preceding updraft as well as the ascent above the density current interface?
- What are the differences in the preceding updraft characteristics between cold-pool-driven outflows compared to RFD-driven outflows, and how can those differences be explained by perturbed environmental factors such as vertical static stability and vertical wind shear?

3. Data & Methods
    a. Observations

This project used data and observations from the Targeted Observations by Radars and Uncrewed aircraft systems of Supercells (TORUS) project, an ongoing research project funded by the NSF and NOAA. The first season of TORUS field operations occurred in May and June of 2019. TORUS deployed in-situ and remote instruments to observe supercell thunderstorms with the goal of improving understanding of supercells and their relationship with various storm-associated boundaries. A NOAA-NSSL mobile Doppler lidar was deployed with the TORUS campaign observing the near-inflow supercell environment, with 17 total deployment days. The lidar's typical scan strategy included a single 70° elevation plan-position indicator (PPI) scan every two minutes with continuous vertically pointed scans, or vertical stares,in between. The PPI scans yield horizontal wind profiles with 18-meter vertical resolution via the velocity-azimuthal display (VAD) method. Vertical stares allow the lidar to directly measure

vertical velocity and sample turbulence characteristics with one second temporal resolution and 18-meter vertical resolution.

During TORUS operations, the mobile Doppler lidar was deployed in advance of the target thunderstorm such that the storm would pass just to the north. In an optimal deployment, this would allow the lidar to first observe the storm's inflow region. Assuming that the lidar was not overtaken by precipitation, the lidar would then observe the storm's density current. In some cases this density current was cold-pool-driven, while in others it was more characteristic of an RFD. The field program which deployed the lidar also included frequent soundings, which can be used to determine environmental wind shear and static stability. In addition to lidar data and soundings, operational Doppler radar data are available for these cases (not shown). The radar data provide important context about the environments in which these density currents were generated and propagate and allow for general understanding of parent storm morphology.

b. Idealized Modeling

To analyze the relationship between density currents and environmental shear and static stability, idealized numerical simulations were performed and compared to field observations. Simulations were completed using the Cloud Model 1 (CM1; Bryan et al. 2003) numerical model. CM1 is a three-dimensional, non-hydrostatic, non-linear, time-dependent numerical model designed for idealized studies of atmospheric phenomena. Simulations were run at the OU Supercomputing Center for Education and Research (OSCER).

The simulations were run in two dimensions, with a 200-km domain in the horizontal and a 15-km domain in the vertical. The horizontal grid spacing was 50 m, while the vertical grid spacing was a constant 25 m below 3 km, with vertically stretching above the 3-km level. Most simulations ran for two hours and output data every 5 minutes. Two high-resolution simulations discussed below output data every 10 seconds. The density current is created using a dam-break initial condition similar to that in Liu and Moncrieff (2000). The 5-km-wide cold block has a prescribed potential temperature perturbation and is placed in the center of the domain. To study the different range of density currents observed during TORUS (e.g, cold pools and RFDs), we created three separate potential temperature perturbation cases that were designed to determine

sensitivity to environmental shear and stability. A control case was defined with a potential temperature perturbation of 6 K. A weaker perturbation of 3 K was used to represent the RFD case. A stronger perturbation of 9 K was used to represent the cold pool. In reality, potential temperature perturbations within the observed thunderstorms likely differed among cold pools and RFDs. Our decision to group simulated RFDs and cold pools by the same potential temperature perturbation allowed us to maintain a reasonable number of simulations for this project.

To determine the environmental shear and stability ranges for the idealized simulations, average environmental shear and static stability were taken of each of the eight observed density current passages during TORUS. Environmental parameters are derived from soundings launched by a mobile far-field team 25-50 km in advance of the storm, and can be found in Table 1. The average field-observed environmental parameters from TORUS informed the different environmental conditions to test across the three potential temperature perturbation cases. By introducing the density current cases into different levels of environmental shear and static stability, we were able to draw comparisons of the impacts of those environmental parameters on the simulated density currents' vertical velocity field. Initial tests of shear magnitudes similar to those observed in the field led to significant downstream advection of cold air from the cold block via the density current's leading updraft as it entered stronger shear. This is an unrealistic effect, which we aimed to limit by implementing smaller shear magnitudes of 2 m s^{-1} (weak shear, or WS), 6 m s^{-1} (moderate shear, or MS), and 10 m s^{-1} (strong shear, or SS) in the environment. Shear was constant throughout the 0-3 km layer, with easterly winds linearly shifting to westerly winds of equal values. Static stability within the shear layer was broken into 1 K km^{-1} (weak lapse rate, or WL), 3 K km^{-1} (moderate lapse rate, or ML), and 5 K km^{-1} (strong lapse rate, or SL). With three levels of shear and stability for each perturbation type, nine total simulations were generated for each of the three perturbations, resulting in 27 total simulations (Fig. 2).

4. Data Analysis
    a. Observations

Analysis of observations collected during the TORUS 2019 field season indicates that there were eight well-defined cases of density current passages directly over the mobile lidar. During TORUS operations, the lidar frequently observed stronger updrafts in advance of the density current than previous studies have shown. Two canonical cases are selected from the eight to represent cold-pool-driven outflow and RFD outflow. The cold-pool-driven outflow case for this study occurred on June 3, 2019 near Boise City, OK, while the RFD-driven case occurred on May 28, 2019 near Imperial, NE (all times UTC). Vertical velocity observations are shown for the cold-pool-driven Boise City case and the RFD-driven Imperial case in Figures 7 and 8, respectively. The density current's passage is shown by the sharp gradient between updraft (positive vertical velocity) and downdraft (negative vertical velocity). In the cold-pool-driven Boise City case, surface passage of the density current occurred at 0059 UTC and passage at 500 meters at 0102 UTC. The RFD-driven Imperial case displayed surface passage at around 0128 UTC and passage at 500 meters at about 0129 UTC. These observations of a sloped density current interface are consistent with previous studies such as Huston et al. (2019). Both density currents experienced strong ascent just prior to density current passage, hereafter referred to as forced ascent.

b. Idealized Simulations

Cross-sections of the 27 simulations are shown in Figures 3 - 5. Here, we show each density current in a steady-state, where the impacts of cold block initialization are minimized, after 40 minutes of simulation. The 40-minute mark represents a point when the simulated density currents are steady-state, with linear propagation speeds, but before most of them had lost their well-defined vertical velocity fields. Our analysis focuses on the region near the density current head. Figure 3 represents strong perturbations (SP), which we intend to be analogous to the cold pool case. Figure 4 represents medium perturbations (MP), meant as a control case. Lastly, Figure 5 represents weak perturbations (WP), intended to model the RFD case.

Strong simulated density currents are evidenced by higher potential temperature perturbations, taller density current heads, and stronger magnitudes of vertical velocity near the density current head. In identical environments, density currents were strongest in the SP

simulations and weakest in the WP simulations. In all perturbation regimes, density current characteristics were variable across the shear and stability parameter space we evaluated. Stronger density currents were favored under less statically stable (WL) and weaker shear (WS) environments. The strongest density current created was the strong-perturbation, weak-lapse, weak-shear (SPWLWS) simulation, while the weakest, essentially nonexistent density current was the weak-perturbation, strong-lapse, strong-shear (WPSLSS) simulation. WL and WS environments tended to promote faster density current propagation, while SL and SS environments tended to promote slower density current propagation.

To provide a comparison between idealized simulations and field observations, Doppler lidar vertical velocity observations are simulated by taking profile time series at a fixed point in the x domain for two simulation cases. One simulated stare is from the SPMLWS case, which represents the environment of the cold-pool-driven Boise City case. The other is from the WPMLSS case, which represents the environment of the RFD-driven Imperial case.

c. Comparison of Simulations to Field Observations

In general, the magnitude of vertical velocities shown around the density current interface in these idealized simulations are smaller than those collected in field observations during TORUS. This difference partially stems from our choice of display time; in using the 40-minute mark in Figures 3-5 to ensure that we had steady-state density currents, vertical velocity magnitudes had lessened as the density currents evolved from their initial forcing. Density currents produced by supercell thunderstorms, which were the parent thunderstorms of the majority of the density current passages observed during TORUS, do not have an initial forcing followed by a slow decline in intensity. As long as the supercell is maintained, density currents can experience near-constant forcing. Furthermore, given that our idealized simulation framework initialized the initial cold block in the middle of the domain, each simulation resulted in two density currents: a slower-propagating density current that moved eastward (the focus of our study), and a faster-propagating density current moving westward. Supercells generally occur in sheared environments that do not promote two density currents propagating in opposite directions. These two factors, in addition to the simulated environment's constant atmospheric

stratification, likely contribute to weaker vertical velocity magnitudes in our idealized simulations compared to TORUS observations.

Vertical velocity around actual thunderstorm density currents are also likely to be less perfectly correlated with decreased shear and decreased static stability than our idealized simulations suggest. Thunderstorms are inherently complex phenomena with complex internal mechanics. The RFD observed at Imperial, NE registered forced ascent of around 15 m s^{-1} shortly before RFD passage, despite having a presumably weaker potential perturbation than the Boise City observed cold pool, which registered forced ascent of around 5 m s^{-1}. Internal thunderstorm dynamics are difficult to resolve within CM, which hinders our ability to draw blanket conclusions of the effect of potential temperature perturbation strength, environmental shear, and environmental static stability on vertical velocity fields around density currents.

However, some density currents simulated within CM1 bear a striking qualitative resemblance to those observed during TORUS. High-resolution simulated stares are given from the SPMLWS and WPMLSS cases in Figures 6 and 7, respectively. These stares are taken from before the 40-minute mark that we defined as steady-state, and thus must be analyzed with the caveat that they are non-steady-state. Simulated density current propagation speeds between the beginning of the simulation and the displayed time are treated as linear, but in reality the density currents had modestly nonlinear speeds, moving faster in the initial release of the cold block than at the time of the simulated stare. We selected earlier times knowing that despite simulated density currents having modestly nonlinear speeds, the faster propagation speeds earlier in the simulations would give us a more complete cross-section of density current passage. Furthermore, the times selected give more visual similarity between simulated and observed stares, allowing us to draw comparisons between simulated and real density currents. The Boise City observed stare and the SPMLWS simulated stare look similar, with a sloped density current structure and accelerating vertical velocity toward the density current head. The observed stare has a slightly taller density current, but both feature forced ascent around halfway between the surface and the top of the density current. Conversely, the Imperial observed stare and the WPMLSS simulated stare appear to share few similarities. While the observed stare features a

rapid density current passage throughout the lowest km and strong forced ascent, the simulated stare features a slow density current passage through the lowest 200 m and weak forced ascent.

Both observed and simulated stares reveal vertical velocity characteristics that are not addressed in the Droegemeier and Wilhemson (year) conceptual model (Fig. 1). First, ascent is noted in the minutes immediately preceding forced ascent at the density current interface. This feature is hereafter referred to as the antecedent updraft. Second, ascent is often maintained above the density current after the passage of the associated surface boundary, which is later referred to as ascent above the density current. These two characteristics are the focus of further investigation.

d. Antecedent Updraft

Noteworthy among field observations during TORUS was the presence of sustained boundary layer ascent in advance of the forced updraft near density current heads. Oftentimes, this ascent lasted on the order of ten minutes, implying a spatial scale of several km. This antecedent updraft is apparent for 10 minutes prior to passage between 0048 and 0058 UTC in the cold-pool-driven Boise City case (Fig. 8) Studies of density currents have noted the forced updraft near density current heads (see Droegemeier and Wilhelmson 1987), but vertical velocity in the region in advance of the density current is less studied.

The high-resolution SPMLWS, which represents a simulated cold pool similar to Boise City, provides evidence of this long-duration antecedent updraft (Fig. 6). At the fixed location, ascent is present within the entire boundary layer 7 minutes prior to the density current passage. The antecedent updraft is stronger aloft than near the surface at this time, and increases as the density current approaches and forced ascent begins. Near the surface, ascent increases more slowly with time, and thus the transition to forced ascent at the density current head is much more dramatic. Given that the fixed location in the SPMLWS case was at x = 15 km, and that the density current began passing at 19 minutes, the density current's average speed within the first 15 minutes was about 13 m s^{-1}. Knowing that, and knowing that the antecedent updraft occurred seven minutes prior to density current passage, it can then be estimated that the antecedent updraft for this simulated case was around 5 km wide.

The cold-pool-driven observed stare from Boise City appears to confirm that this vertical velocity structure of the antecedent updraft occurs in the field, as well. By 0048 UTC, 10 minutes prior to the passage of the density current at the surface, ascent was noted throughout the 400-800 meter layer and would remain that way until the density current had passed. By 0051 UTC, ascent was present throughout the entire lowest kilometer of the atmosphere, except in the lowest 100 meters, where data are noisy. From 0054 to 0057 UTC, vertical velocities in the 300-1000 meter layer showed a marked increase in magnitude, while the lowest 300 meters generally saw a lesser change in vertical velocity. This meant that when the density current head approached, a much more rapid acceleration of ascent occurred near the surface than as the density current head approached aloft, similar to the evolution noted in the simulations. Doppler radar records for the cold pool indicate that it propagated at about 6 m s^{-1}. Knowing that antecedent updraft occurred 10 minutes prior to density current passage, the antecedent updraft for this observed case was estimated to be around 4 kilometers in width.

Antecedent updraft is identified during both real and simulated RFD passages, as well. The WPMLSS high-resolution simulated stare, representing an RFD similar to Imperial, had a sustained antecedent updraft for at least six minutes prior to the passage of the density current. Due to the slow-moving nature of this simulated RFD, the antecedent updraft did not have as large a spatial extent as its temporal extent might suggest . Given that the fixed location in the WPMLSS idealized stare is at x = 4 km, and that the density current began passing at around 16 minutes, the density current's average speed within the first 16 minutes was about 4 m s^{-1}. Taking this propagation speed into consideration, and noting that the antecedent updraft occurred at least six minutes prior to density current passage, we estimate that the antecedent updraft for this case was at least 1.5 kilometers in width.

In the observed RFD-driven Imperial case, four minutes elapsed between the onset of antecedent updraft in the lowest kilometer of the atmosphere and the density current passage at the surface. Forced ascent was very strong in this case, approaching 15 m s^{-1} above 600 meters. Given that there were only four minutes between the onset of antecedent updraft and the beginning of density current passage, vertical velocities rapidly accelerated in the upper boundary layer. Doppler radar analysis shows that the RFD propagated at about 13 m s^{-1}.

Knowing that antecedent updraft occurred 4 minutes prior to density current passage, the antecedent updraft for this observed case was estimated to be around 3 kilometers in width.

Generally speaking, stronger antecedent updrafts were associated with stronger density currents – in other words, density currents with the strongest remaining potential temperature perturbations and strongest forced ascent. However, duration of the antecedent updraft appeared to have a relationship with wind shear in the idealized simulations: stronger vertical velocities generally appeared further ahead of forced ascent at the density current interface in strong-shear simulations (see MPMLSS compared to MPMLWS, for example). Keeping in mind that non-hydrostatic effects can impact the vertical velocity near and ahead of density currents (Wakimoto 1982), there appears to be a relationship between environmental shear and horizontal extent of antecedent updraft in our simulations. Stronger perturbations had a larger spatial extent of antecedent updraft within the simulations (see SPMLMS compared to WPMLMS, for example). Less statically stable simulations allowed antecedent updraft to reach greater heights above the density current head (see SPSLMS compared to SPWLMS, for example).

e. Ascent Above the Density Current

In previous studies covering the conceptual model of density currents, the vertical motions behind the head of the density current are not particularly well-defined. While the conceptual model from Droegemeier and Wilhelmson (Fig. 1) shows some downward motion within the density current itself, there is no mention of motion above the density current interface. In contrast, the observations from both Imperial, NE and Boise City, OK showed a distinct density current interface that separated a general upward motion above the density current and the general downward motion within the density current. This is most easily seen in the Boise City lidar observation, specifically from 0100 to 0105 UTC. The ascent above the density current is also evident in the Imperial observation from 0127 to 0128 UTC, but the observation is hindered by precipitation and the stares being interrupted each minute for the lidar to profile horizontal wind. The ascent above the density current is important because it modifies the environment such that it can impact the parent thunderstorm or help to support new

convection. The spatial and temporal aspects of ascent above the density current can determine how effectively the environment is modified.

In the idealized simulations, this maintained ascent was not as clear, but it did exist. As noted previously, the Boise City, OK lidar observation (Fig. 8) shows persistent ascent along and above the density current interface. Within the high-resolution idealized simulation of the Boise City, OK case (Fig. 9), this feature is less prominent as ascent is mostly focused ahead and on the head of the density current. The ascent above the density current is mitigated by Kelvin-Helmholtz instabilities causing turbulence along the density current interface. There is also weak environmental subsidence post-boundary passage. This subtle difference is likely attributed to limitations of our 2-D model framework, and differences between the environmental conditions of the idealized simulation and the real-life observation (most notably wind shear due to the model framework).

The main attribute contributing to the difference in the structure of the density current interface is the difference in the amount of turbulence behind the leading edge of the density current. In the idealized simulation, there were issues with Kelvin-Helmholtz instabilities behind the density current boundary that created high magnitude updrafts and downdrafts which broke down the density current interface. This occurs when the density current begins to reach its steady state condition about 15 minutes into the simulation. In the SPMLWS simulation (Fig. 3), the head of the density current is tall, but narrow because of the mixing behind the leading edge of the density current. In the Boise City, OK lidar observation, while turbulence behind the boundary is evident, the density current interface is clear as there is general upward motion above the density current, and general downward motion within it. Simulations with weaker cold blocks exhibited less of this turbulence allowing for the updraft to be more uniform, although it should be noted these updrafts were weaker. This is best shown in the high-resolution WPMLSS case where, because of the slower forward speed of the density current, it is easier to observe the structure of the density current and the uniformity of the updraft above it. Because of the weaker perturbation, the mixing of the environment and the denser air from the cold block was much less turbulent, thus, the density current interface was more intact.

5. Summary & Discussion

The TORUS 2019 field campaign provided opportunities for researchers to observe density currents with a mobile Doppler lidar. While in the field, researchers noted that boundary layer ascent began in the minutes preceding forced ascent along the density current interface. Additionally, on occasion researchers noted the ascent continued unabated above shallow density currents following the passage of the leading edge. This work used CM1 idealized simulations to explore the sensitivity of the antecedent updraft and ascent above the density current to density current strength and environmental parameters. To do so, we conducted simulations with three different potential temperature perturbations, with each perturbation regime encountering environments with three different levels of shear and static stability.

Our simulations indicated that vertical velocities are stronger near the density current interface when the initial potential temperature perturbation is stronger, atmospheric static stability is lower, and environmental shear is weaker. Such results should be tempered with the knowledge that our simulations did not attempt to resolve thunderstorm dynamics, which can lead to far different results in reality. Comparing the observed Imperial RFD case to the observed Boise City cold pool case shows this - the RFD had vertical velocities three times the magnitude of the cold pool.

However, our simulations did feature the antecedent updraft and ascent above the density current interface. In both observed and simulated cases, the antecedent updraft and ascent above the density current lasted on the order of minutes, suggesting spatial extents on the order of kilometers. This reaches into the mesoscale, and suggests that both antecedent updrafts and ascent above density currents may serve as mesoscale areas of lift. Mesoscale areas of lift and their contributions to convection initiation, maintenance, and storm morphology continue to be a focal point of scientific research (e.g., Wu 2016 and Shapiro et al. 2018). These two areas of lift are not accounted for in the classic conceptual model of density current structure (Droegemeier and Wilhemsen 1987). It is important for scientists to continue to observe and research antecedent updraft and ascent above the density current to understand their role in boundary layer evolution and convective processes in near-storm environments.

It is important to note that our study was based on a limited sample of density current passages collected during the TORUS 2019 field campaign. To truly understand the relationship between the features we identified and potential temperature perturbation strength, environmental shear, and environmental static stability, a much larger sample of density current passages would need to be considered. Furthermore, our method of grouping observed potential temperature perturbations was qualitative – RFDs were grouped, and cold pools were grouped. In reality, not all RFDs have the same potential temperature perturbation, and not all cold pools have the same potential temperature perturbation. A more accurate quantification of potential temperature perturbation within observed density currents would allow for more specific conclusions about density current type and mesoscale lifting behaviors.

Our study was also limited by the ability of our chosen 2D model framework to represent a thunderstorm density current. Using the dam break method, our simulated density currents had a cold potential temperature perturbation of similar shape and a vertical velocity field similar to observed density currents. However, we did not create a constant forcing to maintain that density current such as would be expected within a thunderstorm. Therefore, to more accurately compare observed and simulated density currents, we used simulated stare times before the density currents could reliably be considered steady-state. This may have affected the linearity of the density currents' propagation speed, and opened our vertical velocity profiles to non-hydrostatic effects. On the whole, we still expect that the times chosen allow for an accurate comparison between observed and simulated density currents.

Future research in this area is necessary to better understand the relationship between density currents and the near-storm environment. Further observations of potential temperature perturbations of varying magnitudes, and within different environmental shear and static stability, will help firm our understanding of how those perturbations and conditions can impact antecedent updraft and ascent above density currents. Further modeling work is necessary to determine the impacts both antecedent updraft and updraft above density currents may have on storm-scale dynamics, as well as its effectiveness as a source of mesoscale lift in the generation and sustenance of convection. This will help us understand the importance of these two features within density current and storm conceptual models.

6. Acknowledgments

We thank the National Severe Storms Laboratory and the TORUS field campaign participants for allowing us to use their observations for this research. We also thank the OU Supercomputing Center for Education & Research (OSCER) at the University of Oklahoma for providing us the resources for the computing for this project.

7. Reference List

Bryan, G. H., J. C. Wyngaard, and J. M. Fritsch, 2003: Resolution requirements for the simulation of deep moist convection. *Mon. Wea. Rev.*, **131**, 2394–2416.

Bryan, G. H., and R. Rotunno, 2014b: The optimal state for gravity currents in shear. *J. Atmos. Sci.*, **71**, 448–468.

Byers, H., and R. Braham, 1949: The Thunderstorm. *United States Government Print Office*.

Charba, J., 1974: Application of gravity current model to analysis of squall-line gust front.*Mon. Wea. Rev.*, **102**, 140–156.

Crum, T. D., Alberty, R. L., & Burgess, D. W., 1993: Recording, archiving, and using WSR-88D Data. *Bull. Amer. Meteor. Soc.*, **74**, 645–653.

Droegemeier, K. K., & Wilhelmson, R. B., 1985a: Three-Dimensional Numerical Modeling of Convection Produced by Interacting Thunderstorm Outflows. Part I: Control Simulation and Low-Level Moisture Variations. *J. Atmos. Sci*, **42**, 2381–2403.

Droegemeier, K. K., & Wilhelmson, R. B., 1987: Numerical simulation of thunderstorm outflow dynamics. Part I: outflow sensitivity experiments and turbulence dynamics.*J. Atmos. Sci.*, **44**, 1180–1210.

Goff, R. C., 1976: Vertical structure of thunderstorm outflows. *Mon. Wea. Rev.*, **104**, 1429–1440.

Gunter, W. S., J. L. Schroeder, and B. D. Hirth, 2015: Validation of dual-Doppler wind profiles with in situ anemometry. *J. Atmos. Sci.*, **32**, 943–960.

Hutson, A., C. Weiss, and G. Bryan, 2019: Using the Translation Speed and Vertical Structure of Gust Fronts to Infer Buoyancy Deficits within Thunderstorm Outflow. *Mon. Wea. Rev.*, **147**, 3575–3594.

Lee, B. D., & Wilhelmson, R. B., 1997b: The Numerical Simulation of Nonsupercell Tornadogenesis. Part II: Evolution of a Family of Tornadoes along a Weak Outflow Boundary. *J. Atmos. Sci.*, **54**(19), 2387–2415.

Liu, C., & Moncrieff, M. W, 2000. Simulated density currents in idealized stratified environments. *Monthly Weather Review*, 128, 1420-1437.

Markowski, P. M., J. M. Straka, and E. N. Rasmussen, 2002: Direct surface thermodynamic observations within the rear-flank downdrafts of nontornadic and tornadic supercells. *Mon. Wea. Rev.*, **130**, 1692–1721.

Martner, B. E., 1997: Vertical Velocities in a Thunderstorm Gust Front and Outflow. *J. Appl. Meteor. Climatol.*, **36**, 615–622.

Reif, D. W., and H. B. Bluestein, 2019: An Analysis of the Vertical Velocity at the Leading Edge of a Density Current During PECAN. *18th Conference on Mesoscale Processes*.

Rotunno, R., J. B. Klemp, and M. L. Weisman, 1988: A theory for strong, long-lived squall lines. *J. Atmos. Sci.*, **45**, 463–485.

Seigel, R. B., and S. C. V. D. Heever, 2012: Simulated Density Currents beneath Embedded Stratified Layers. *J. Atmos. Sci.*, **69**, 2192–2200.

Shapiro, A., E. Fedorovich, and J. G. Gebauer, 2018: Mesoscale Ascent in Nocturnal Low-Level Jets. *Journal of the Atmospheric Sciences*, **75**, 1403–1427.

Simpson, J. E., 1969: A comparison between laboratory and atmospheric density currents. *Quart. J. Roy. Meteor. Soc.*, **95**, 758–765.

Straka, J. M., Wilhelmson, R. B., Wicker, L. J., Anderson, J. R., & Droegemeier, K. K., 1993: Numerical solutions of a non-linear density current: A benchmark solution and comparisons. *Int. J. Numer. Methods Fluids*, **17**, 1–22

Wakimoto, R. M., 1982: The Life Cycle of Thunderstorm Gust Fronts as Viewed with Doppler Radar and Rawinsonde Data. *Mon. Wea. Rev.*, **110**, 1060–1082.

Wilson, J. W., 1986: Tornadogenesis by Nonprecipitation Induced Wind Shear Lines. *Mon. Wea. Rev.*, **114**, 270–284.

Wu, M., and Y. Luo, 2016: Mesoscale observational analysis of lifting mechanism of a warm-sector convective system producing the maximal daily precipitation in China mainland during pre-summer rainy season of 2015. *Journal of Meteorological Research*, **30**, 719–736.

8. Tables

Case	5/20	5/23	5/23	5/24	5/27	**5/28**	5/28	**6/3**	Avg	Avg	Avg
Cold Pool (CP) or RFD	CP	RFD	CP	RFD	RFD	**RFD**	CP	**CP**	CP	RFD	—
0-3km change in theta (K)	7	13	12	7	4	**9**	9	**8**	9	8.25	8.63
0-3km shear (kt)	42	41	44	17	27	**43**	43	**18**	39	32	35.5

Table 1: Environmental shear and static stability within the 0-3km layer for eight observed density current passages used in this study. The bolded dates are the Imperial, NE RFD and Boise City, OK cold pool respectively.

9. Figures

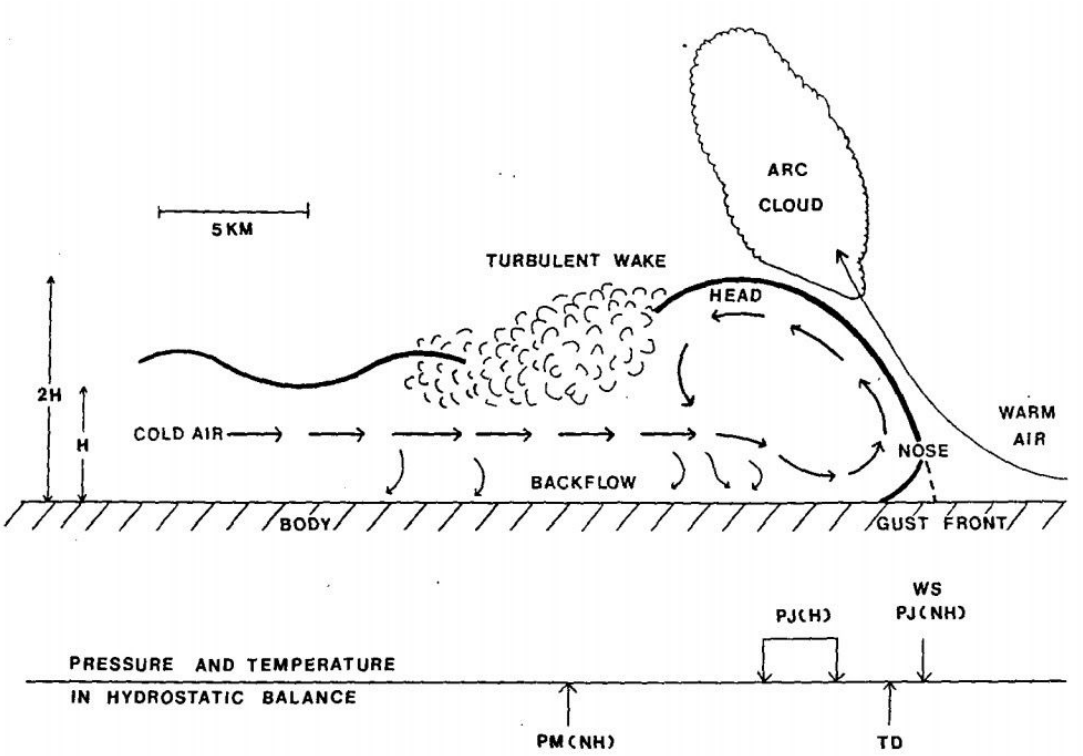

Figure 1: Classic conceptual model of a density current (Wilhelmson and Droegemeier, 1987).

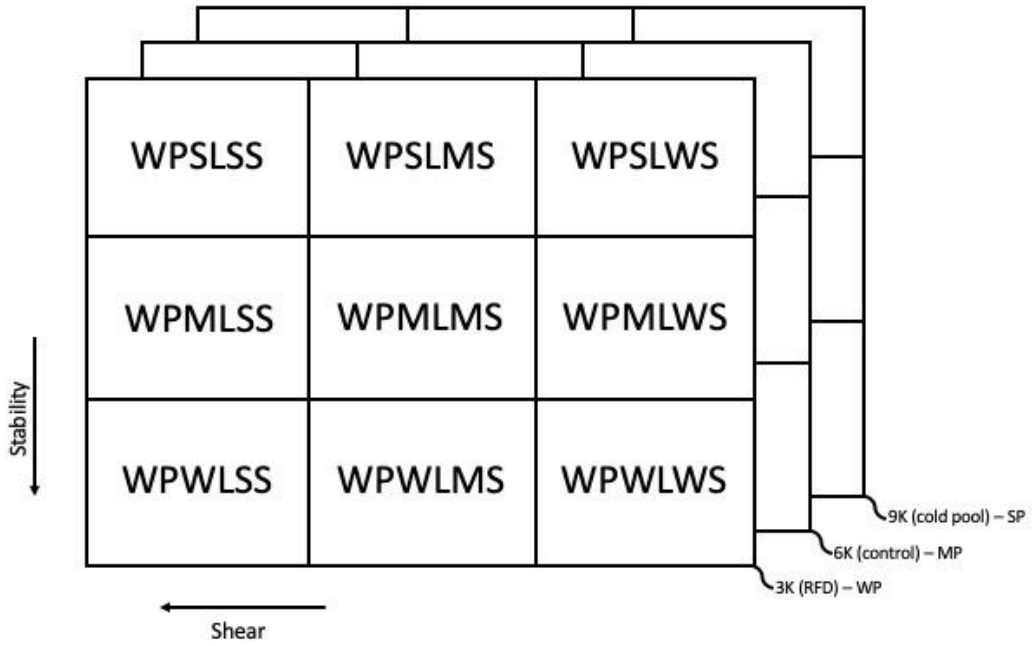

Figure 2: This diagram shows how the parameter space we evaluate breaks down into 9 simulations per perturbation regime. Simulations evaluate 3 levels of environmental shear (decreasing shear along the x-axis) and 3 levels of environmental stability (decreasing stability along the y axis). This 9-simulation framework is duplicated for each perturbation regime represented by successive panes.

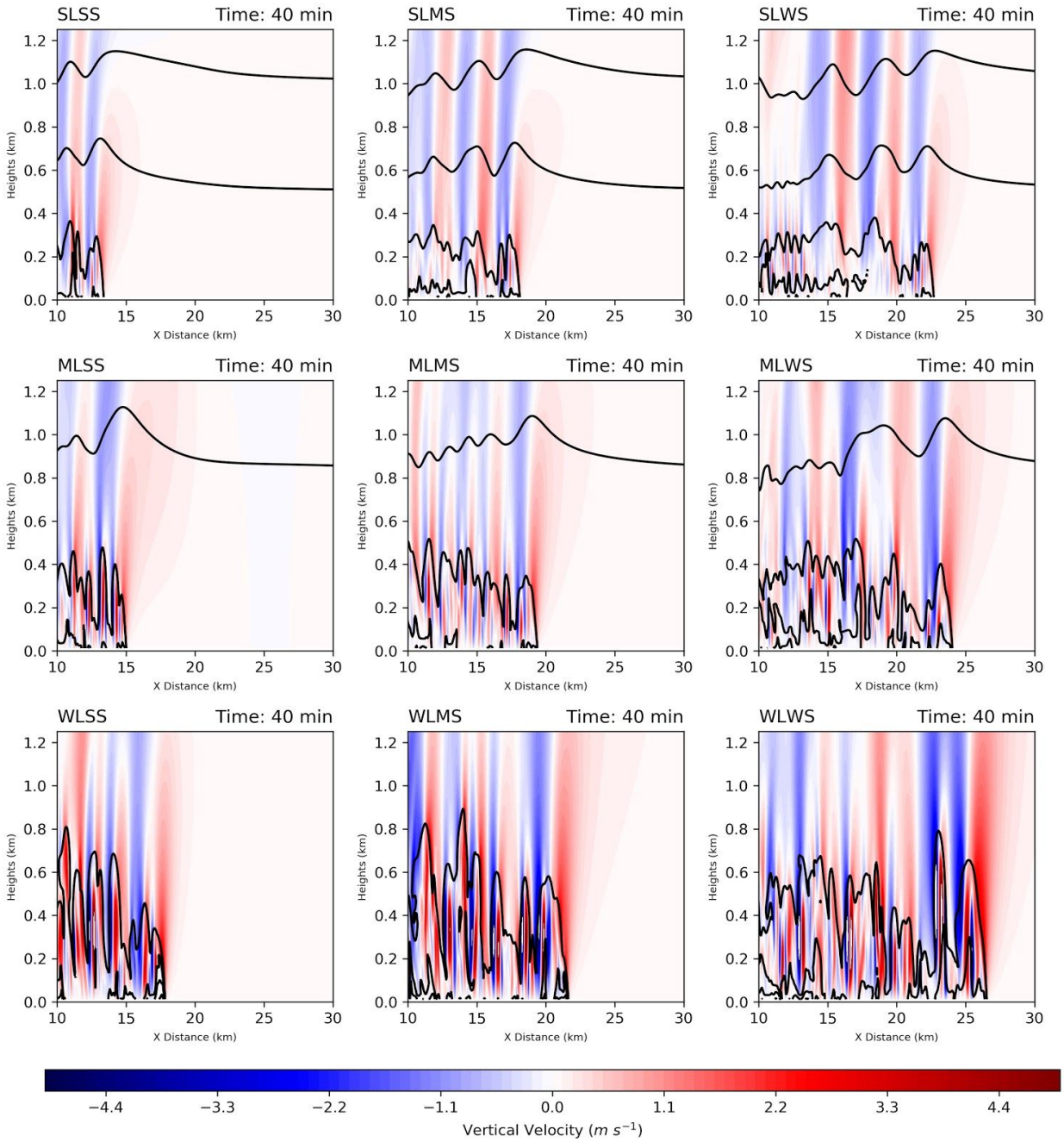

Figure 3: The 9 simulations with the initial cold block temperature perturbation at -9 K (strong perturbation - SP). Along each of the columns, the simulations have a decreasing environmental potential temperature lapse rate (SL → WL). Along each of the rows, the simulations have decreasing environmental wind shear (SS → WS). Colors show direction and magnitude of vertical motions (red = ascent; blue = descent). Black contours show constant lines of potential temperature.

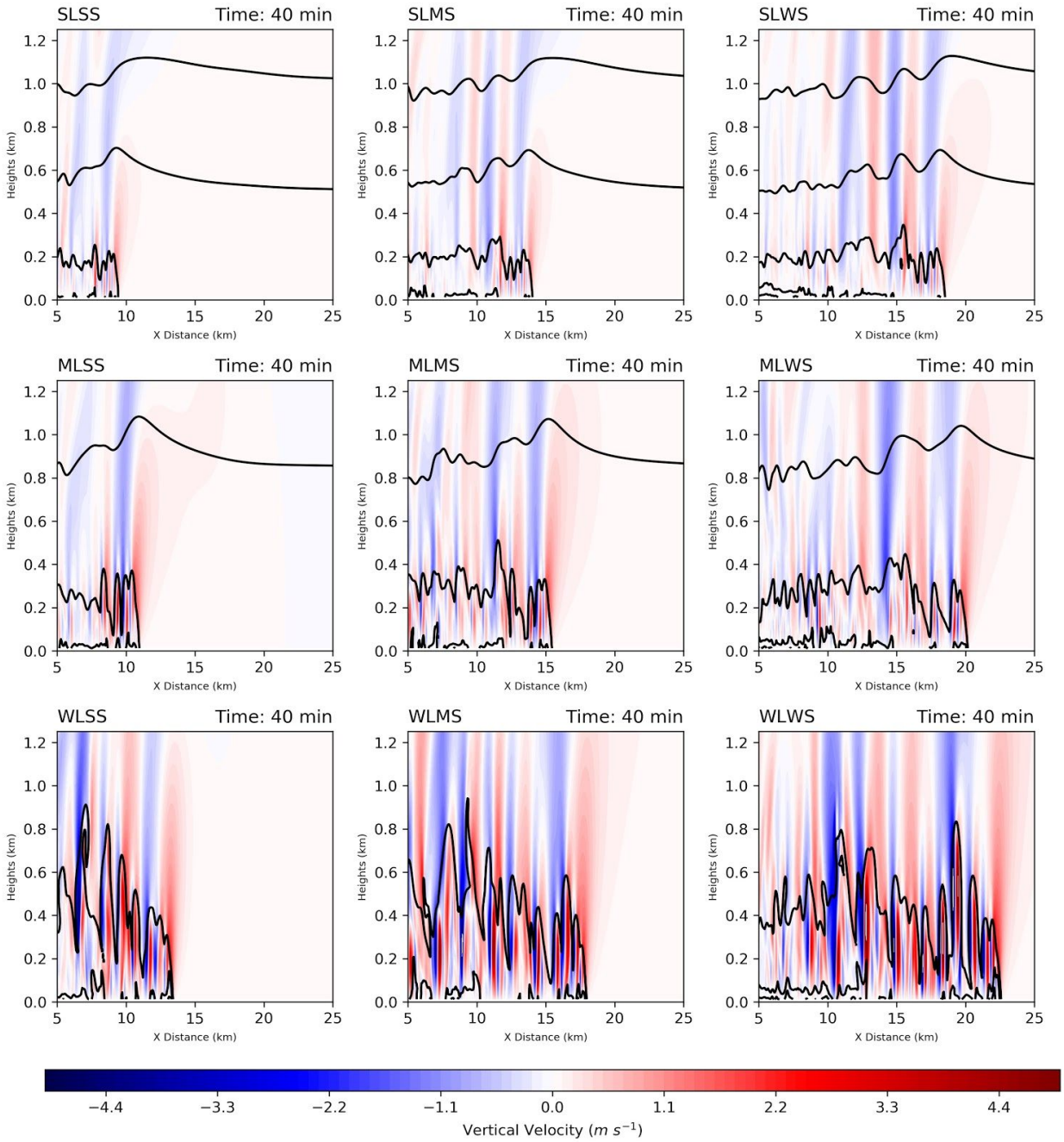

Figure 4: As in Fig. 3, but for an initial cold block potential temperature perturbation of -6 K (moderate perturbation - MP).

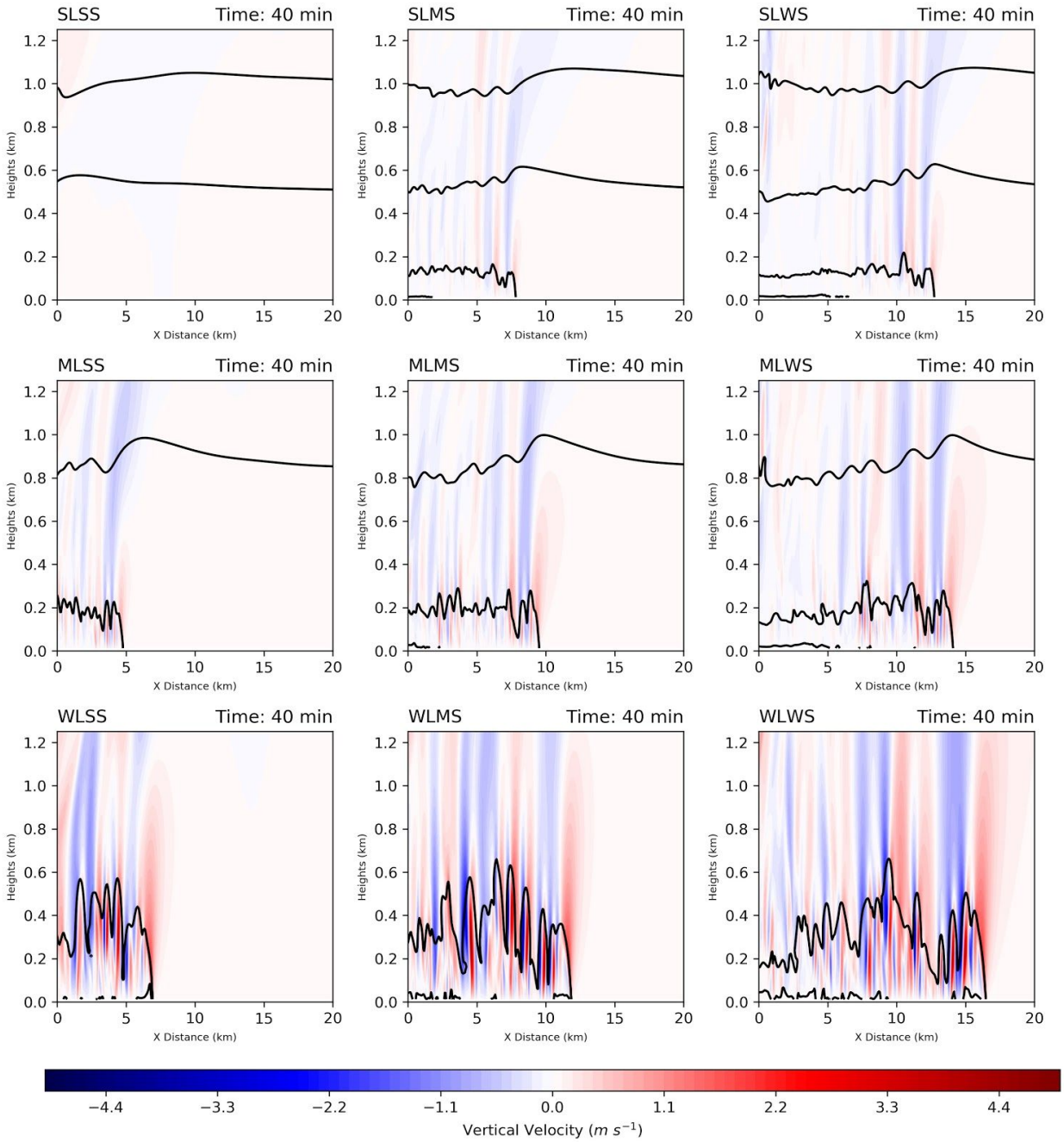

Figure 5: As in Fig. 3, but for an initial cold block potential temperature perturbation of -3 K (weak perturbation - WP).

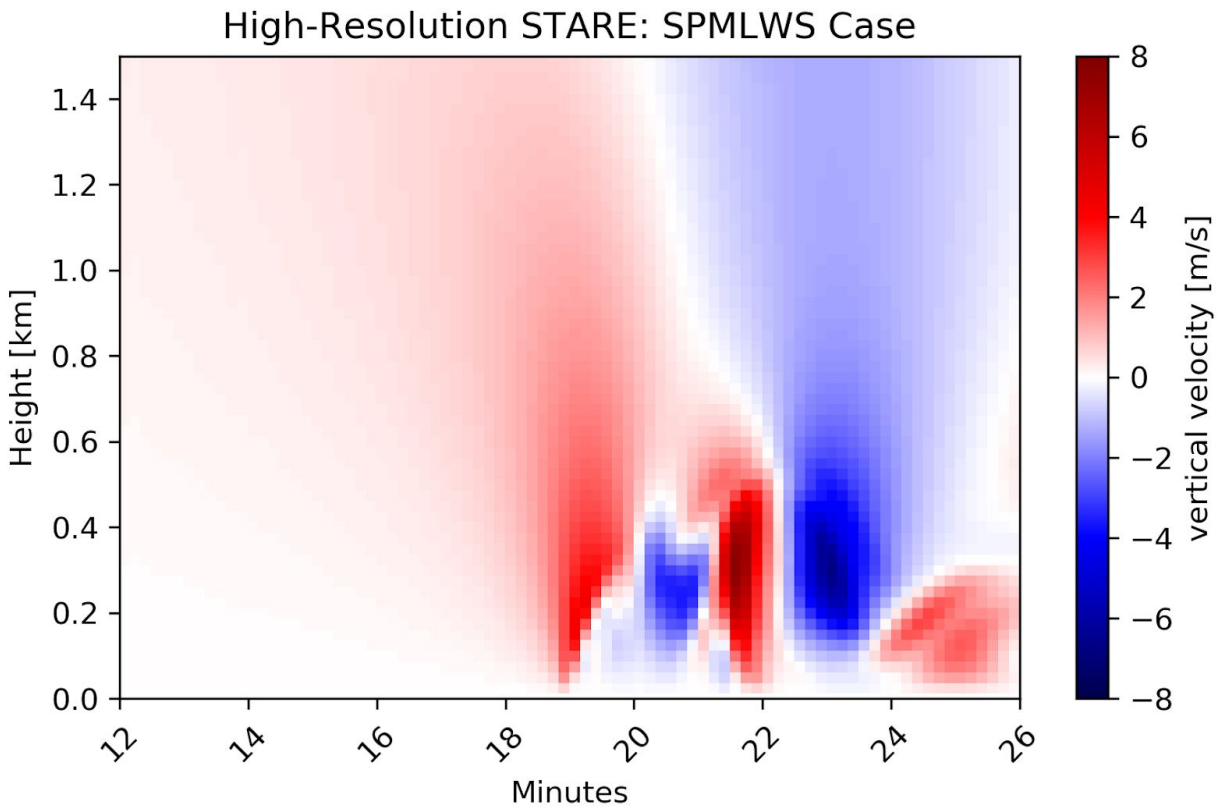

Figure 6: Simulated high-resolution stare from the strong perturbation - medium potential temperature lapse rate - weak shear simulation. These environmental conditions closely represent those observed from the TORUS field campaign on June 2, 2019 in Boise City, Oklahoma.

Figure 7: Simulated high-resolution stare from the weak perturbation - medium potential temperature lapse rate - strong shear simulation. These environmental conditions closely represent those observed from the TORUS field campaign on May 27, 2019 in Imperial, Nebraska.

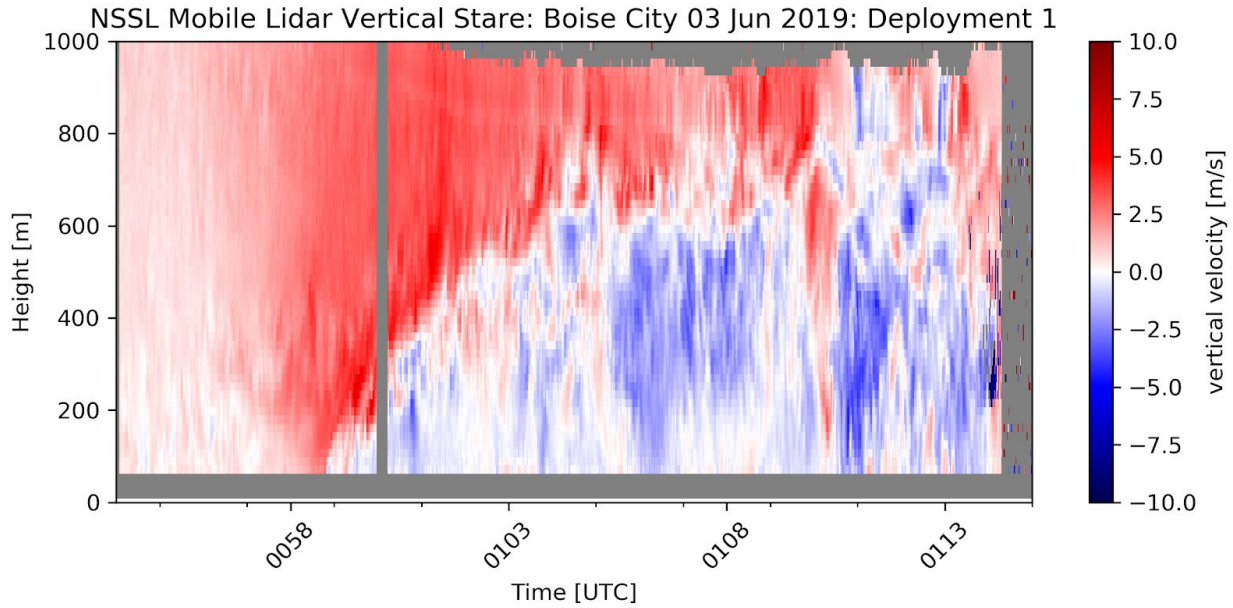

Figure 8: The vertical velocity observation from the NSSL Mobile Doppler Lidar from Boise City, Oklahoma.

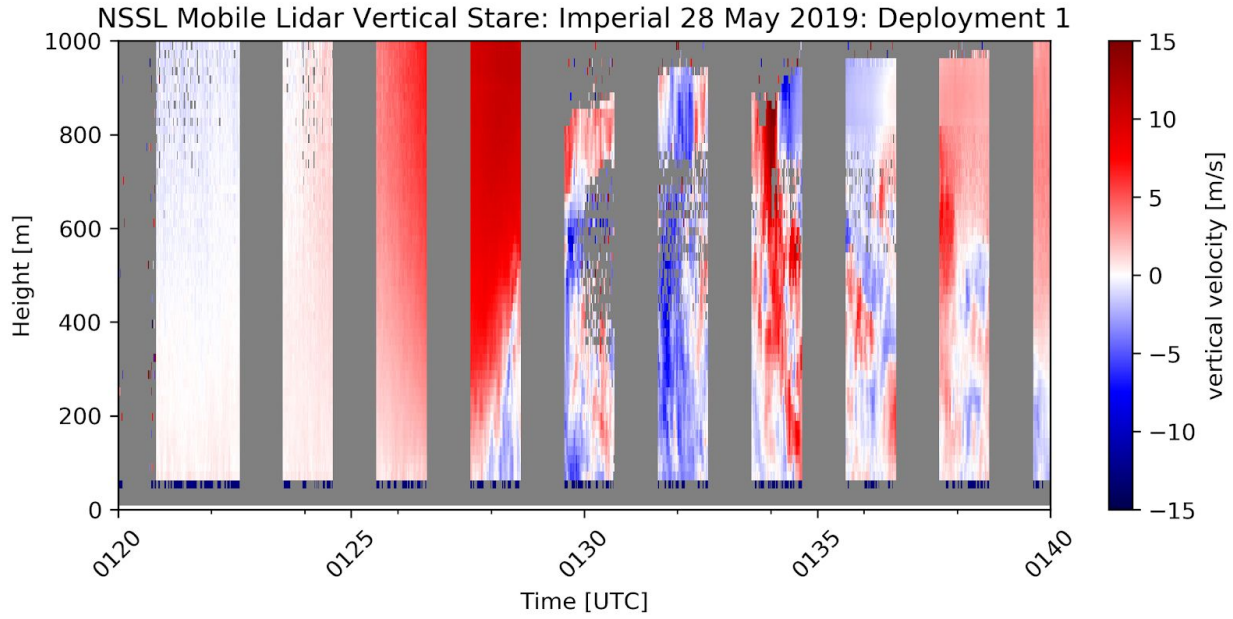

Figure 9: The vertical velocity observation from the NSSL Mobile Doppler Lidar from Imperial, Nebraska. Missing data is from the Mobile Doppler Lidar's time conducting VAD scans of the environment.